Heliyon 10 (2024) e32029

Contents lists available at ScienceDirect

Heliyon

journal homepage: www.cell.com/heliyon

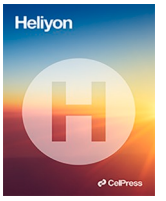

Review article

Structure-properties correlation of acrylic resins modified with silver vanadate and graphene

Beatriz Danieletto Sahm [a], Izabela Ferreira [a], João Marcos Carvalho-Silva [a], Ana Beatriz Vilela Teixeira [a], Jean Valdir Uchôa Teixeira [b], Paulo Noronha Lisboa-Filho [b], Oswaldo Luiz Alves [c], Andréa Cândido dos Reis [a,*]

[a] Departament of Dental Materials and Prosthesis, Ribeirão Preto School of Dentistry, University of São Paulo (USP), Ribeirão Preto, SP, Brazil
[b] Paulista State University Júlio de Mesquita Filho (UNESP), Bauru, SP, Brazil
[c] Department of Inorganic Chemistry, Institute of Chemistry, State University of Campinas (UNICAMP), Campinas, Brazil

ARTICLE INFO

Keywords:
Acrylic resin
Graphene
Mechanical properties
Antimicrobial activity

ABSTRACT

This study aimed to incorporate β-$AgVO_3$ and rGO into self-curing (SC) and heat-curing (HC) acrylic resins and to evaluate their physicochemical, mechanical, and antimicrobial properties while correlating them with the characterized material structure. Acrylic resin samples were prepared at 0 % (control), 0.5 %, 1 %, and 3 % for both nanoparticles. The microstructural characterization was assessed by scanning electron microscopy (SEM) (n = 1) and energy dispersive X-ray spectroscopy (EDS) (n = 1). The physicochemical and mechanical tests included flexural strength (n = 10), Knoop hardness (n = 10), roughness (n = 10), wettability (n = 10), sorption (n = 10), solubility (n = 10), porosity (n = 10), and color evaluation (n = 10). The microbiological evaluation was performed by counting colony-forming units (CFU/mL) and cell viability (n = 8). The results showed that the β-$AgVO_3$ samples showed lower counts of *Candida albicans*, *Pseudomonas aeruginosa*, and *Streptococcus mutans* due to their promising physicochemical properties. The mechanical properties were maintained with the addition of β-$AgVO_3$. The rGO samples showed higher counts of microorganisms due to the increase in physicochemical properties. It can be concluded that the incorporation of β-$AgVO_3$ into acrylic resins could be an alternative to improve the antimicrobial efficacy and performance of the material.

1. Introduction

Since the discovery of the monolayer atomic structure of graphene [1] and the intercalation of silver nanoparticles (AgNPs) into other compounds [2–5], numerous applications have been found in automotive, engineering, and biomedical sciences such as restorative medicine and dentistry [1–5]. Researchers aimed to integrate these biomaterials into dental devices to improve their mechanical and microbiological performance [6,7]. Also, biomaterials including chitosan [8] and carbon fibers [9] were used for this purpose; however, silver and graphene compounds are preferred for their antimicrobial properties, strength, flexibility, and stability when incorporated into biomaterials [6,7].

AgNPs reduce microbial adhesion and disorganize biofilms through direct contact and the release of silver ions [6,7,10–12]. They

* Corresponding author. Department of Dental Materials and Prosthodontics Ribeirão Preto Dental School FORP-USP. Av. Do Café, s/n 14040-904, Ribeirão Preto, SP, Brazil.
E-mail address: andreare73@yahoo.com.br (A. Cândido dos Reis).

https://doi.org/10.1016/j.heliyon.2024.e32029
Received 10 January 2024; Received in revised form 26 April 2024; Accepted 27 May 2024
Available online 28 May 2024

also induce microbial death by generating reactive oxygen species (ROS) and altering membranes [6,7,10–12]. However, due to the challenge of obtaining agglomeration-free AgNPs, Holtz et al. [13] developed nanostructured beta-vanadate decorated with silver nanoparticles (β-$AgVO_3$). This compound stabilizes the AgNPs and exhibits antimicrobial activity by interacting with cellular proteins, thiol groups of microbial enzymes, and inhibiting DNA replication [6,13,14]. The use of β-$AgVO_3$ at low concentrations (0.5 %–5 %) in dental materials confers antimicrobial activity, reduces local and systemic infections, and maintains their mechanical performance [6].

Similar to AgNPs, graphene tends to agglomerate, which reduces its microbial activity [7]. For this reason, the chemical modification of reduced graphene oxide (rGO) is proposed by reducing its agglomeration, oxidation, and cytotoxicity while increasing its conductivity due to the higher presence of carbon bonds [7]. Due to the reduced amount of oxygen in rGO, ROS activity is reduced [15]. However, its antimicrobial activity is maintained by electron transfer and the nano-knife capacity of its sharp-edged surface, which alters the bacterial osmotic pressure and leads to the disruption of its cell membrane [7,15–18].

β-$AgVO_3$ and rGO can induce cytotoxicity at high concentrations through interaction with cell membranes, generation of oxidative stress, induction of immune responses, and enhanced release of Ag and V ions and C fragments [13,19–22]. However, the synthesis of these materials at the nanometer scale reduces their cytotoxic potential, as low concentrations are effective as antimicrobials [13,19,20]. β-$AgVO_3$ exhibits high stability and controlled release of Ag and V ions, and rGO has a lower concentration of O, which reduces its toxic potential against human cells [19–23]. Concentrations of β-$AgVO_3$ between 0.5 and 5 % were not toxic to human gingival fibroblasts [19,24], and less than 4 μg/mL of rGO were not toxic to eukaryotic cells [22,23,25–27].

The acrylic resin utilized in fabricating temporary and definitive dental prostheses, as well as orthodontic and occlusal devices, exhibits surface roughness [28–30]. The roughness and the development of pores during improper polymerization facilitate the adhesion of microorganisms, the formation of biofilms, and the longevity of these devices [31]. *Candida albicans* and *Streptococcus mutans* are the main microorganisms isolated from this material in the oral cavity [32]. They are associated with the development of fungal infections (local and systemic) and dental caries, respectively [32].

In addition, *C. albicans* and *S. mutans* have an affinity for co-aggregation in biofilms [32]. When combined with *Staphylococcus aureus*, they form biofilms with a higher potential for adhesion to dental materials and virulence factors [32]. These microorganisms have also been co-isolated in other types of infections, such as periodontal diseases, urinary tract infections, skin burns, and lung infections [33]. The presence of *Pseudomonas aeruginosa* in *Candida* spp. biofilms demonstrates an antagonistic relationship through competition for nutrients (iron), and the induction of virulence mechanisms to eliminate the fungi [34,35]. However, the association of these microorganisms aggravates systemic infections [34,35].

Modification of resins with nanomaterials can reduce and avoid these failures, although there are challenges with incorporation [36,37]. This material modification can reduce its mechanical effectiveness [36,37] due to the difficulty of homogeneous incorporation of the nanoparticles, as well as reduce the antimicrobial effect because they are not uniformly dispersed over the surface of the material [6,38,39].

In view of the promising characteristics of β-$AgVO_3$ and rGO nanoparticles [3–5,19,20,36–43], this study aimed to determine which of the nanomaterials would improve the antimicrobial performance and physico-mechanical properties of the resins. The novelty of this study is the incorporation of rGO into acrylic resins due to its molecular stability in the reduced compound.

2. Material and methods

2.1. Synthesis of β-$AgVO_3$ and rGO

The synthesis of β-$AgVO_3$ was performed as previously described by Holtz et al. [13] by precipitation reaction between silver nitrate ($AgNO_3$, Merck 99.8 %) and ammonium metavanadate (NH_4VO_3, Merck 99 %).

rGO was synthesized using the modified Hummers' method, as developed by Abdolhosseinzadeh et al. [44], employing a solution comprising graphite, potassium permanganate ($KMnO_4$), sulfuric acid (H_2SO_4), and glucose as a reducing agent.

2.2. Characterization of β-$AgVO_3$ and rGO

Characterization was performed by transmission electronic microscopy (TEM) and X-ray diffraction (XRD) at room temperature using a Shimadzu XRD-7000 diffractometer with Cu Kα radiation (λ = 1.5406 Å), 40 kV, and 30 mA. Data were collected continuously from $10^\circ < 2\theta < 60^\circ$ at a rate of 2° per minute. Fourier transform infrared (FTIR) spectroscopy was also performed, where the samples were diluted and formed into tablets using analytical grade potassium bromide (KBr), and then Fourier transform infrared spectra were collected using transmittance from 4000 to 400 cm^{-1} region.

2.3. Determination of the minimum inhibitory concentration (MIC)

The MIC was determined by the serial dilution method in duplicate, as described by the Clinical and Laboratory Standards Institute (CLSI) [45]. The *C. albicans* strain (ATCC 10231) was cultured on Sabouraud Dextrose (SD) agar and then inoculated into SD broth. The *S. mutans* (ATCC 25175), *S. aureus* (ATCC 25923), and *P. aeruginosa* (ATCC 27853) strains were separately inoculated into Brain Heart Infusion (BHI) broth. The inocula were cultured in a microbiological oven (DeLeo, B2DG, Bento Gonçalves, Rio Grande do Sul, Brazil) at 37 °C until exponential growth. The culture was then centrifuged at 6000 rpm for 5 min, the supernatant was discarded, and the pellet was washed twice in phosphate-buffered saline (PBS) containing NaCl, KCl, Na_2HPO_4, and KH_2PO_4. The *C. albicans* inoculum was standardized (to approximately $1x10^6$ CFU/mL) by counting in a Neubauer chamber (HBG, Gießen, Germany) coupled to a light

microscope (Axio Observer A1, Carl Zeiss, Jena, Germany). The bacterial inoculum was standardized (to approximately $1x10^7$ CFU/mL) using a spectrophotometer (Multiskan GO; Thermo Scientific, Waltham, MA, USA) with an absorbance reading of 0.150 nm at a wavelength of 625 nm.

A 96-well plate was prepared by inoculating 100 μL of culture medium at a concentration of $1x10^6$ (*C. albicans*) and $1x10^7$ (bacteria) CFU/mL, respectively. A solution of β-$AgVO_3$ and rGO powders in sterilized distilled water was prepared at a concentration of 1000 μg/mL, and 100 μL was added to the first well (500 μg/mL) and homogenized. Successive dilutions were made by transferring 100 μL of the suspension to the next well, so that the concentration of the β-$AgVO_3$ and rGO solutions was reduced by half with each dilution. Ten concentrations of antimicrobials were obtained, as well as a positive control (inoculated culture medium and PBS) and a negative control (culture medium and β-$AgVO_3$ and rGO solutions). The plate was incubated at 37 °C and after 48 (*C. albicans*) and 24 h (bacteria), the microbial growth was assessed by the turbidity of the sample with the naked eye. An aliquot of the plate wells was seeded into a Petri dish to confirm the MIC.

2.4. Specimen preparation

The specimens were made by adding metal matrices of the same shape and size for each test in a conventional metal muffle (OGP, Dental Products Ltda., São Paulo, SP, Brazil). The powder of Dencôr Lay (Clássico®, Art. Clássico, São Paulo, SP) self-curing and heat-curing resins was weighed to determine the amount of nanomaterial to be added. Previous results showed that the addition of 0.5–3% of nanomaterials to polymers is effective against biofilms and does not induce changes in the physicochemical and mechanical properties [19,20]. Therefore, these concentrations were subtracted from the weight of the resins, and then the nanomaterials were added as described in Table 1.

The powders were incorporated into the self-curing (SC) monomer liquid (DMT polymerization inhibitor methacrylate monomer) and the heat-curing (HC) monomer (topanol methacrylate monomer) according to the manufacturer's recommended ratio. Subsequently, the resins were added into molds (plastic phase) and compressed in metal muffles using a hydraulic press (Protecni Hydraulic Press, Protecni Equip. Med., Araraquara, SP, Brazil) at 1000 Kgf for 60 min. Subsequently, the HC groups were polymerized in a water bath using a heat-curing machine at 65 °C for 1 h, followed by a stage at 100 °C for 30 min.

After obtaining the HC and SC samples containing β-$AgVO_3$ and rGO, they were stored free of moisture for 24 h, polished, and then used for the tests. For the flexural strength test, 140 specimens (65 mm × 10 mm x 3.3 mm) were prepared according to ISO 20795–1:2008 (n = 10). For SEM, EDS, roughness, hardness, and wettability tests, 280 samples (9 mm × 2 mm) were obtained (n = 10 for mechanical and physicochemical tests and n = 2 for microstructural analysis). And 448 samples (15 mm × 2 mm) for sorption, solubility, and porosity, and 448 samples (6 mm × 10 mm x 3.3 mm) for microbiological colony-forming unit (CFU/mL) and cell viability tests.

2.5. Microstructural characterization of the samples

The samples were characterized by scanning electron microscopy (SEM) and energy dispersive X-ray spectroscopy (EDS). A thin layer of gold was coated on the samples prior to evaluation. The analysis was performed using an FEI Magellan 400 L microscope equipped with an EDS system for surface chemical characterization.

2.6. Evaluation of antimicrobial activity

The CFU counts of *C. albicans*, *S. mutans*, *S. aureus*, and *P. aeruginosa* were performed after biofilm formation on the acrylic resin specimens modified with β-$AgVO_3$ and rGO. Biofilm formation was initiated by placing the acrylic resin samples into 24-well plates without additional adhesion methods, followed by the addition of 1500 μL of SD broth (for *C. albicans*) and BHI broth (for bacteria) inoculated with the respective microbial strains. Subsequently, the plates were incubated for 1 h and 30 min at 37 °C with 75 rpm

Table 1
Composition of acrylic resins incorporated with nanomaterials.

Composition (% mass)
Resin HC (control group 0 %)
Resin HC + 0.5 % β-$AgVO_3$
Resin HC + 1 % β-$AgVO_3$
Resin HC + 3 % β-$AgVO_3$
Resin HC + 0.5 % rGO
Resin HC + 1 % rGO
Resin HC + 3 % rGO
Resin SC (control group 0 %)
Resin SC + 0.5 % β-$AgVO_3$
Resin SC + 1 % β-$AgVO_3$
Resin SC + 3 % β-$AgVO_3$
Resin SC + 0.5 % rGO
Resin SC + 1 % rGO
Resin SC + 3 % rGO

agitation for the microbial adhesion phase. The culture medium was then removed, the samples were washed with 2 mL of PBS, and 1500 mL of the appropriate culture medium was added for microbial growth. The plates were then incubated for 48 h at 37 °C with 75 rpm agitation for biofilm maturation.

After biofilm formation, the samples were washed with PBS and transferred to polypropylene tubes containing 10 mL of PBS. Each tube was serially diluted by adding 25 μL to microtubes containing 250 μL of PBS. Serial dilutions from 100 to 10^{-3} were obtained, and aliquots of 25 μL were plated on Petri dishes containing SD agar (for *C. albicans*), cetrimide agar (for *P. aeruginosa*), salt mannitol agar (for *S. aureus*), and SB20 agar (for *S. mutans*). The plates were then incubated for 24 h at 37 °C, with *S. mutans* incubated under microaerophilic conditions.

After this period, the CFU count was performed according to equation (1):

CFU/10 mL = (number of colonies x $10^{n/q}$) x 10 Equation 1

where n is the absolute value of the dilution and q is the amount in mL pipetted for each dilution when seeding the plates. In this study, $q = 0.025$ refers to 25 μL of each dilution.

The cell viability of the biofilm formed on the SC and HC samples was assessed in triplicate (n = 8) using the XTT cell viability kit (Uniscience, São Paulo, Brazil) prepared according to the manufacturer's instructions. Aliquots of 100 μL from the polypropylene tubes and 50 μL of XTT solution [2,3-bis-(2-methoxy-4-nitro-5-sulfophenyl)-2H-tetrazolio-5-carboxanilide] were added to 96-well plates. The plates were then incubated at 37 °C for 2 h in the dark, and the absorbance was read on a microplate spectrophotometer (Multiskan GO; Thermo Scientific, Waltham, MA, USA) at a wavelength of 492 nm.

2.7. Evaluation of physicochemical and mechanical properties

2.7.1. Flexural strength

The flexural strength was performed on a universal testing machine (EMIC DL 2000, São José dos Pinhais, Paraná, Brazil) at a speed of 5 mm/min and a load of 20 Kgf.

2.7.2. Microhardness

Microhardness measurements were conducted using a microhardness tester (Shimadzu HMV-2000, Japan). Three random measurements were taken on each specimen utilizing a Knoop-type penetrator with a load of 25 gf applied for 5 s.

2.7.3. Roughness

Roughness was assessed using a 3D laser confocal microscope (LEXT 4000; Olympus, Hamburg, Germany) with a 20× objective lens (MPLAPON). Three measurements were taken per sample, and the total average Sa [μm] parameters were used.

2.7.4. Wettability

The sessile drop method was applied using distilled water by a goniometer (KSV CAM200) with the software (CAM 200 Contact Angle Measurement System). Distilled water was used because it is similar in polarity to human saliva. Each surface received 1 drop of 4 μL and waited 60 s for the drop to stabilize and the average angle (Θ) to be measured as a function of time. Three drops were used per sample, and the disks were dried with a stream of nitrogen for 1 min between analyses.

2.7.5. Sorption, solubility, and porosity

For sorption, solubility, and porosity, the specimens were weighed immediately after being obtained, placed in a desiccator with dehydrated blue silica gel, and weighed daily until the masses were stable (±0.001g), obtaining the initial mass (M1).

For sorption and solubility, they were immersed in 100 mL of distilled water for 7 days until the final mass was obtained (M2) and weighed daily until stability (±0.001 g) (M3).

The mass loss was expressed in g/cm^2 and calculated using equations (2) and (3):

Sorption = M2-M1 (g/cm^2)/V . Equation 2

Solubility = M1-M3 (g/cm^2)/V . Equation 3

For porosity, the specimens were weighed, immersed in 100 mL of distilled water, and then calculated according to equation (4):

Porosity = (volume of dry specimen/volume of wet specimen) x 100% Equation 4

2.7.6. Color evaluation

The color change of SC and HC samples was evaluated using a portable spectrophotometer (Multiskan GO, Thermo Scientific, Multiskan Spectrum, MA, USA) based on CIE-Lab* standards [46]. The ΔE value was calculated using equation (5):

$$\Delta E* = \sqrt{(L*0 - L0)2 + (A*0 - A*)^2 + (B*0 - b*)^2} \quad \text{Equation 5}$$

2.8. Statistical analysis

The data obtained were subjected to statistical analysis using SPSS 20.0 software. ANOVA and post hoc Tukey tests were performed for all tests, except for color evaluation, where Kruskal-Wallis and post hoc Dunn tests were performed ($P < 0.05$).

3. Results

3.1. Characterization of β-$AgVO_3$ and rGO

TEM showed β-$AgVO_3$ crystals with acicular geometry (needle-shaped), an average diameter of 100 nm, and a length of micrometric order, with metallic spheres (approximately 35 nm) decorating the nanowire surfaces (Fig. 1A). TEM also showed the aggregation of rGO flakes (with an individual diameter below 100 nm), demonstrating the degree of compaction of the synthesized particles (Fig. 1B).

The X-ray diffractogram showed the formation of β-$AgVO_3$, indexed by the crystallographic sheet (JCPDS 29–1154) [13,14], and the crystallinity index was estimated at 67 % and the amorphous phase at 33 % (Fig. 2A). The X-ray diffractogram of rGO contains the characteristic planes of the material, which are 002 and 100 at 23° and 42.9°, respectively (Fig. 2B). Based on these planes, the average rGO crystallite size was calculated using the Scherrer equation, with the height per sheet at 0.4 nm, the crystallite height at 1.2 nm, the average length at 22.1 nm, and the number of layers at 3.1.

For β-$AgVO_3$, FTIR showed bands between 400 and 1000 cm^{-1} (attributed to the bonds between the oxygen and vanadium atoms) and a band at 1633 cm^{-1} (corresponding to the vibration of the –OH bond in the water molecule) (Fig. 2C). To confirm the formation of β-$AgVO_3$, the band at 1409 cm^{-1} (attributed to the symmetric N–H deformation) present in the spectrum of the NH_4VO_3 precursor disappeared in the spectrum of β-$AgVO_3$. For rGO, FTIR showed characteristic vibrational bands between 3600 cm^{-1} and 2800 cm^{-1}, indicating the presence of hydroxyls remaining in the structure as well as those adsorbed from moisture (Fig. 2D). There is also the presence of CO_2 derived from the environment, as indicated by the red rectangle between 2200 cm^{-1} and 2500 cm^{-1}. Furthermore, bands at 1500 cm^{-1} and 1750 cm^{-1} were observed, which refer to the vibrations of the interactions between the C–C carbon chains and the C–O oxygenated groups. Finally, there is the presence of a large band between 1000 cm^{-1} and 1200 cm^{-1}, referring to the vibration between the carbon and oxygen atoms remaining in the material.

3.2. Minimum inhibitory concentration (MIC)

The results obtained for the MIC of β-$AgVO_3$ and rGO are shown in Table 2 rGO had no MIC against the microorganisms evaluated (*C. albicans*, *P. aeuroginosa*, *S. aureus*, and *S. mutans*).

3.3. Microstructural characterization of samples

The SEM images showed the presence of small agglomerates in the β-$AgVO_3$ groups at concentrations of 0.5 and 3 % HC (Fig. 3). A higher roughness surface was visually observed for rGO groups compared to the groups containing β-$AgVO_3$, particularly in the HC resin (Fig. 4). Table 3 shows the chemical elements (wt%) present in HC and SC samples with β-$AgVO_3$ and rGO.

3.4. Evaluation of antimicrobial activity

3.4.1. Candida albicans

For SC samples, β-$AgVO_3$ reduced the CFU count of *C. albicans* compared to the other groups (control and rGO) ($P < 0.05$). The addition of 3 % β-$AgVO_3$ showed lower counts for SC and HC samples compared to the other groups ($P < 0.001$). Incorporation of 0.5 % β-$AgVO_3$ into HC showed lower CFU counts compared to 0.5 % rGO ($P = 0.020$) (Fig. 5).

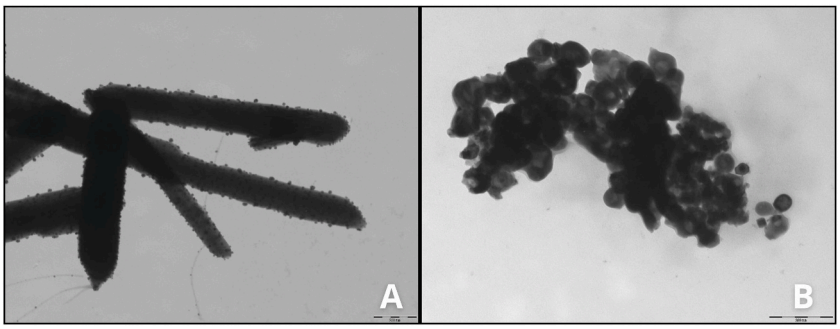

Fig. 1. Transmission electron microscopy (TEM) images (200 nm). A. β-$AgVO_3$; B. rGO.

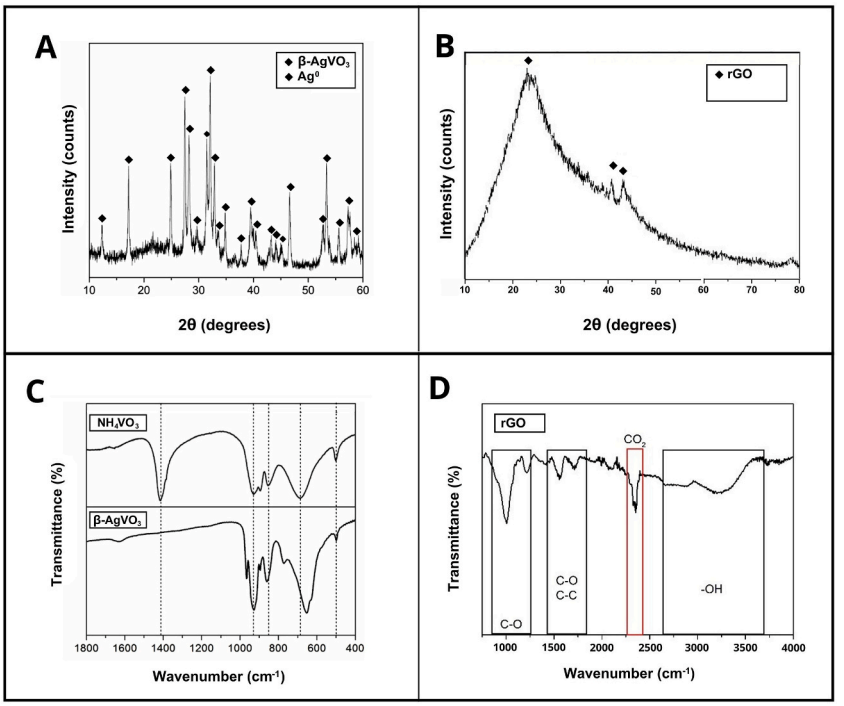

Fig. 2. Structural characterization of nanomaterials. A. X ray diffraction of β-$AgVO_3$; B. X ray diffraction of rGO; C. Fourier transform infrared (FTIR) spectroscopy of β-$AgVO_3$; D. FTIR spectroscopy of rGO.

Table 2
MIC of β-$AgVO_3$ and rGO against C. *albicans*, *P. aeuroginosa*, *S. aureus* e *S. mutans.*

Concentration mg/mL				
Nanomaterials	*C. albicans*	*P. aeuroginosa*	*S. aureus*	*S. mutans*
β-AgVO3	**0,23**	**0,05**	**0,23**	**0,93**
rGO	-	-	-	-

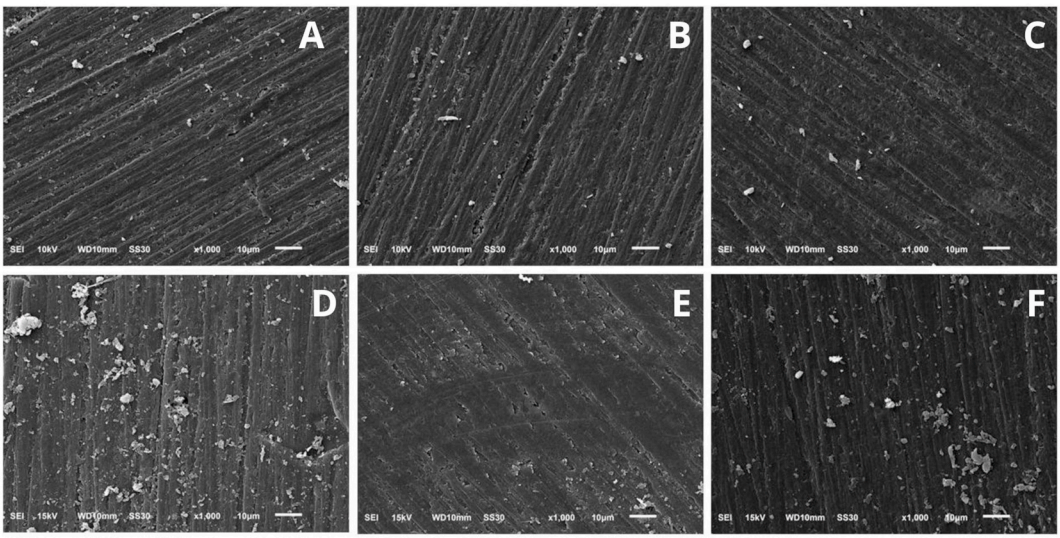

Fig. 3. SEM images of the surface of the samples incorporated with β-$AgVO_3$. A. 0.5 % β-$AgVO_3$ self-curing (SC); B. 1 % β-$AgVO_3$ SC; C. 3 % β-$AgVO_3$ SC; D. 0.5 % β-$AgVO_3$ heat-curing (HC); E. 1 % β-$AgVO_3$ HC; F. 3 % β-$AgVO_3$ HC.

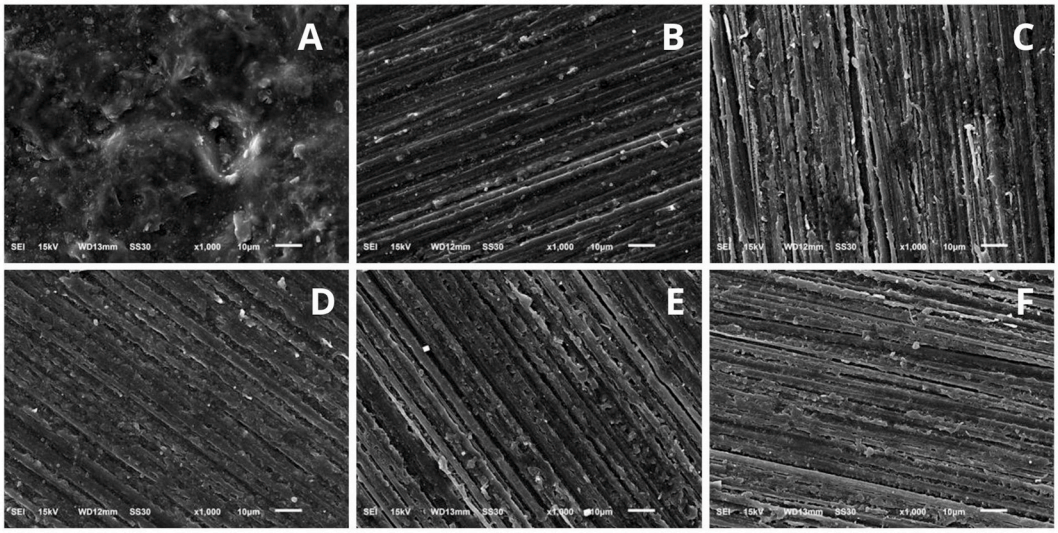

Fig. 4. SEM images of the surface of the samples incorporated with rGO. A. 0.5 % rGO self-curing (SC); B. 1 % rGO SC; C. 3 % rGO SC; D. 0.5 % rGO heat-curing (HC); E. 1 % rGO HC; F. 3 % rGO HC.

Table 3
Results of the chemical elements present in the acrylic resins modified with β-$AgVO_3$ and rGO.

Weight percentagem (%)				
Samples	C	O	V	Ag
Self-cured	58.05	41.95	–	–
0.5 % β-$AgVO_3$	56.16	43.83	0.01	0.00
1 % β-$AgVO_3$	57.38	42.57	0.05	0.00
3 % β-$AgVO_3$	56.72	41.73	0.42	1.13
0.5 % rGO	67.26	32.74	–	–
1 % rGO	69.48	30.52	–	–
3 % rGO	66.55	33.45	–	–
Heat-cured	56.45	43.55	–	–
0.5 % β-$AgVO_3$	54.80	44.86	0.15	0.19
1 % β-$AgVO_3$	58.00	41.94	0.05	0.01
3 % β-$AgVO_3$	57.45	42.21	0.13	0.21
0.5 % rGO	67.78	32.22	–	–
1 % rGO	67.18	32.82	–	–
3 % rGO	66.88	33.12	–	–

3.4.2. Pseudomonas aeruginosa

For HC samples, the 3 % β-$AgVO_3$ had lower CFU count compared to other HC groups ($P < 0.05$). The 1 % β-$AgVO_3$ HC reduced the CFU count of *P. aeruginosa* compared to the rGO groups ($P < 0.05$). Also, for the SC samples the incorporation of 1 % β-$AgVO_3$ reduced the CFU count of *P. aeruginosa* compared to the 0.5 % rGO ($P = 0.054$), 1 % rGO ($P = 0.048$), and 3 % rGO ($P = 0.37$) groups (Fig. 5).

3.4.3. Staphylococcus aureus

There was no reduction in *S. aureus* colony counts ($P > 0.05$) (Fig. 5).

3.4.4. Streptococcus mutans

For SC and HC samples, the 3 % β-$AgVO_3$ group showed the lower CFU count compared to the other β-$AgVO_3$ and rGO groups ($P < 0.05$). Regarding SC, the 1 % β-$AgVO_3$ group reduced the *S. mutans* count compared to the control group ($P = 0.023$). Similarly, in HC, the 1 % β-$AgVO_3$ group reduced the *S. mutans* count compared to the control ($P = 0.001$). Incorporation of rGO did not affect the CFU count compared to the control group for both resins ($P > 0.05$) (Fig. 5).

3.4.5. Cell viability

There was a decrease in the metabolic activity of the *C. albicans* biofilm formed on the 1 % and 3 % β-$AgVO_3$ samples and the 0.5 % and 1 % rGO samples ($P < 0.05$). There was also a decrease in the metabolic activity of the *P. aeruginosa* biofilm formed on the HC samples containing 1 % ($P = 0.035$) and 3 % ($P = 0.000$) β-$AgVO_3$. No decrease in metabolic activity was observed for *C. albicans*, *S. aureus* and *S. mutans* biofilms formed in HC and for *P. aeruginosa*, *S. aureus* and *S. mutans* biofilms formed in SC (Fig. 6).

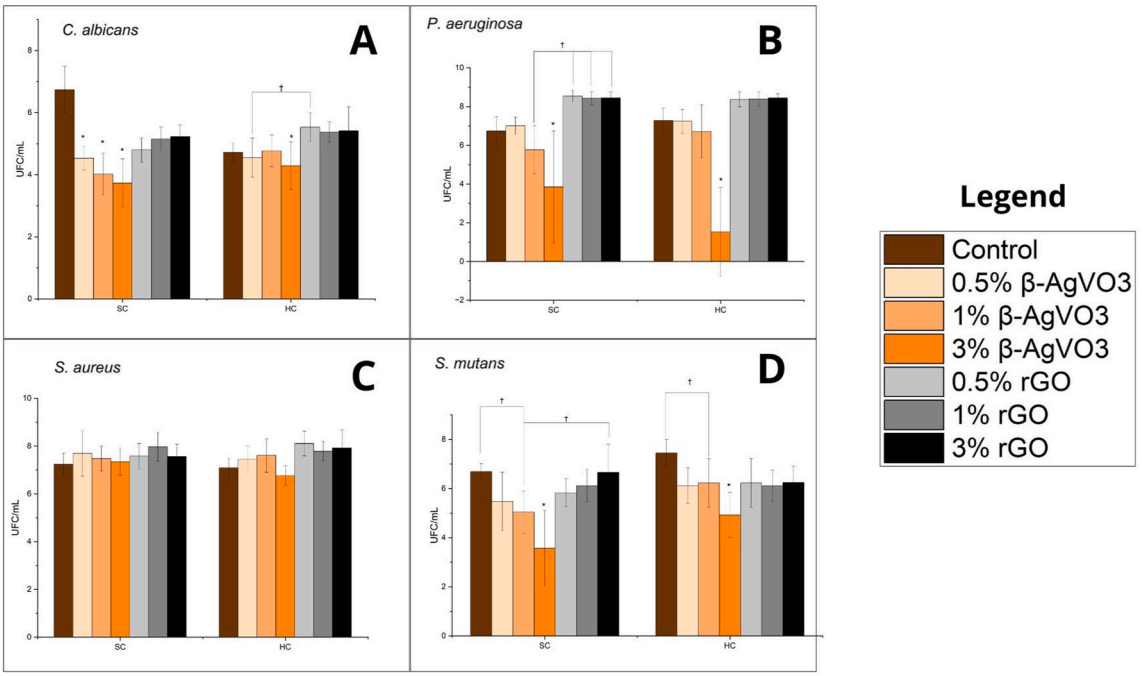

Fig. 5. Mean and standard deviation of CFU/mL counts of microorganisms in acrylic resins incorporated with β-$AgVO_3$ and rGO. A. *Candida albicans*; B. *Pseudomonas aeruginosa*; C. *Staphylococcus aureus*; D. *Streptococcus mutans*. Legend: * statistical difference for all groups and † difference between the indicated groups.

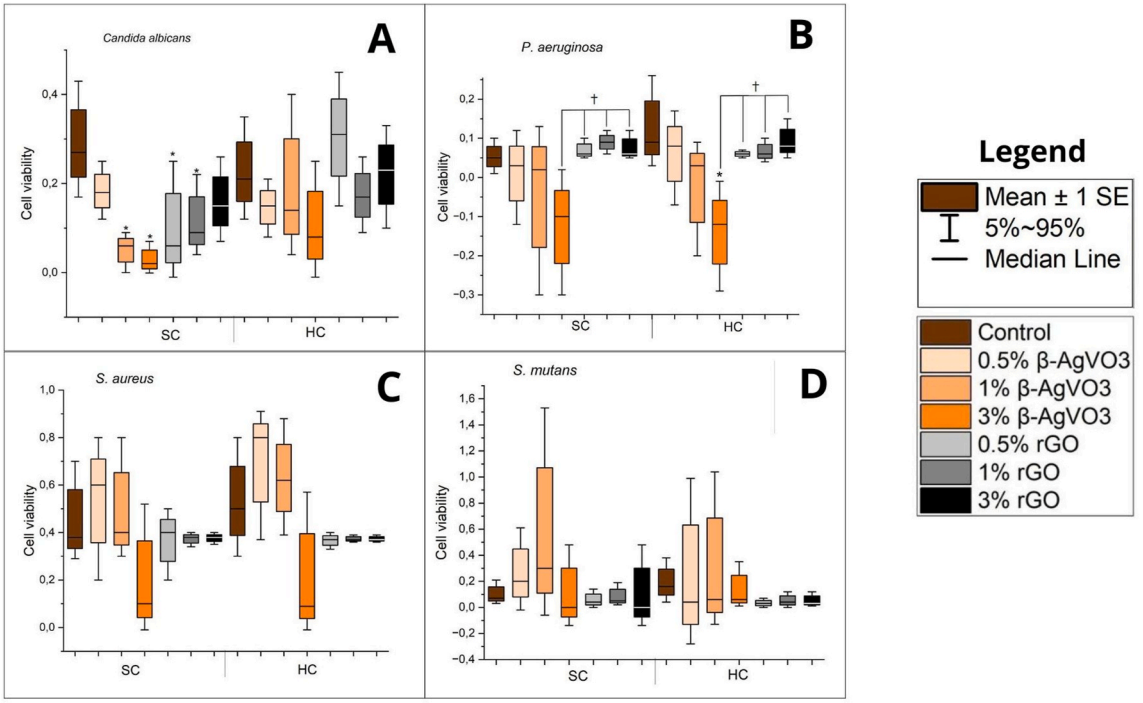

Fig. 6. Median values and confidence intervals of cell viability of biofilms formed in acrylic resins incorporated with β-$AgVO_3$ and rGO. A. *Candida albicans*; B. *Pseudomonas aeruginosa*; C. *Staphylococcus aureus*; D. *Streptococcus mutans*. Legend: * statistical difference for all groups and † difference between the indicated groups.

3.5. Physico-chemical and mechanical properties

3.5.1. Flexural strength

The mean and standard deviation values for flexural strength are shown in a graph (Fig. 7). The incorporation of β-$AgVO_3$ did not affect the flexural strength of the SC control, regardless of the concentration incorporated ($P > 0.05$). The incorporation of 0.5 % rGO increased the flexural strength of SC resin ($P < 0.001$), and this group showed higher flexural values than the other groups ($P = 0.000$).

The 1 % rGO-SC group showed similar flexural strength to the groups with β-$AgVO_3$ and control group ($P > 0.05$), except for 0.5 % β-$AgVO_3$. The 3 % rGO-SC group showed the lowest flexural strength, with a statistical difference compared to the other groups ($P < 0.05$).

Incorporation of rGO into HC resin significantly reduced flexural strength compared to the other groups ($P < 0.001$). Furthermore, the incorporation of β-$AgVO_3$ into HC resin did not affect the flexural strength ($P > 0.000$).

3.5.2. Microhardness

Incorporation of different concentrations of β-$AgVO_3$ does not affect the hardness of SC and HC resins ($P > 0.05$) (Fig. 8).

The incorporation of rGO increased the hardness values of the SC resin, and the group with 0.5 % rGO was the one with the highest hardness values and a statistical difference in relation to the other groups ($P < 0.05$). The groups with 1 % and 3 % rGO in the SC resin showed higher hardness than the 0 % control groups and the groups with β-$AgVO_3$ incorporation $P < 0.05$), but there was no statistical difference between them ($P > 0.05$).

The different concentrations of rGO increased the hardness values of the HC samples ($P > 0.05$) with statistical differences in relation to the HC control and the β-$AgVO_3$ groups $P < 0.05$).

3.5.3. Roughness

The 1 % β-$AgVO_3$ group had less roughness compared to the 3 % rGO group ($P < 0,05$). Incorporating rGO in the three concentrations evaluated (0.5, 1, and 3 %) increased the roughness of the SC samples ($P < 0,05$) (Fig. 9). The incorporation of 3 % β-$AgVO_3$ and 0.5 % and 3 % rGO increased the roughness of the HC resin ($p < 0.05$).

3.5.4. Wettability

For SC samples, the incorporation of 0.5 % and 1 % rGO did not change their wettability ($P > 0.05$) (Fig. 10). However, the 3 % rGO made the surface more hydrophilic compared to the control ($P = 0.001$). In addition, the 1 % and 3 % β-$AgVO_3$ groups presented a more hydrophilic surface compared to the control and rGO groups ($P < 0.05$). The 0.5 % β-$AgVO_3$ group also showed the most hydrophilic surface ($P < 0.001$).

For HC samples, the β-$AgVO_3$ and rGO groups reduced the contact angle of water with the surface ($P < 0.05$). The 0.5 % and 1 % β-$AgVO_3$ groups and the rGO groups showed similar wettability ($P > 0.05$). In contrast, the 3 % β-$AgVO_3$ and rGO reduced the contact angle of water with the resin surface, making the surface more hydrophilic than the other groups $P < 0.05$).

3.5.5. Sorption, solubility, and porosity

The incorporation of 1 % and 3 % rGO resulted in an increase in sorption, solubility, and porosity for both the SC and HC groups ($P < 0.05$) (Table 4). In contrast, the incorporation of 1 % and 3 % β-$AgVO_3$ decreased these properties for SC and HC resins ($P < 0.05$). The incorporation of 0.5 % β-$AgVO_3$ and 0.5 % rGO did not affect the sorption, solubility, or porosity of the SC and HC groups ($P > 0.05$).

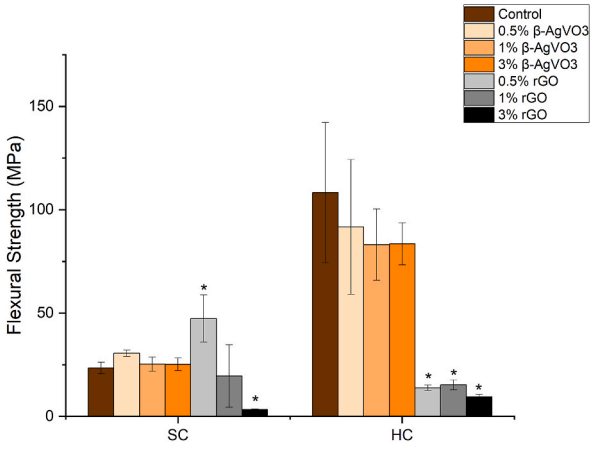

Fig. 7. Mean values and standard deviation of flexural strength of acrylic resins incorporated with rGO and β-$AgVO_3$. Legend: * statistical difference for all groups.

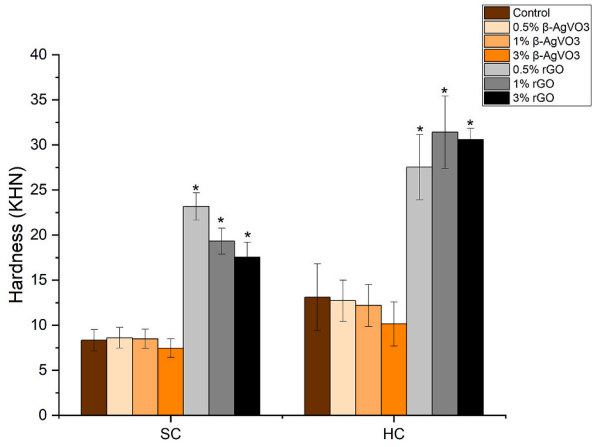

Fig. 8. Mean values and standard deviation of the hardness of acrylic resins incorporated with rGO and β-$AgVO_3$. Legend: * statistical difference for all groups.

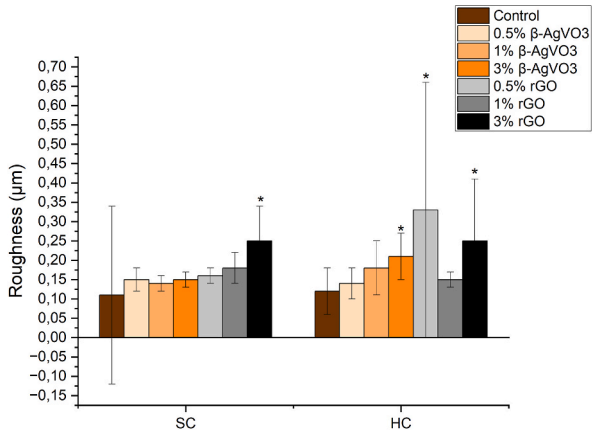

Fig. 9. Mean values and standard deviation of the roughness of acrylic resins incorporated with rGO and β-$AgVO_3$. Legend: * statistical difference for all groups.

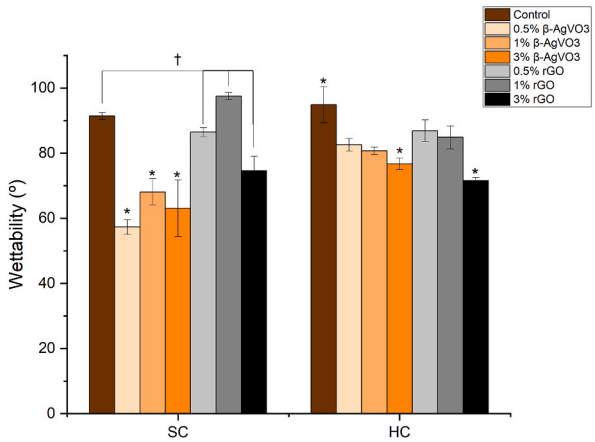

Fig. 10. Mean values and standard deviation of the wettability of acrylic resins incorporated with rGO and β-$AgVO_3$. Legend: * statistical difference for all groups.

Table 4
Mean values and standard deviation of sorption, solubility and porosity of acrylic resins incorporated with β-AgVO3 and rGO.

Groups	Sorption and Solubility	Porosity
Resin SC (0 %)	$2.13 \pm 0.29^{C,D,L,O}$	$2.12 \pm 0.28^{F,N,O}$
0.5 % β-AgVO$_3$	$2.11 \pm 0.23^{C,E,G}$	$2.11 \pm 0.26^{E,F,H,I}$
1 % β-AgVO$_3$	$1.74 \pm 0.33^{F,H}$	$1.76 \pm 0.34^{G,J,K}$
3 % β-AgVO$_3$	$1.52 \pm 0.34^{F,J,K}$	$1.52 \pm 0.38^{G,L,M}$
0.5 % OGr	$2.11 \pm 0.33^{D,E,I,M}$	2.12 ± 0.29^{E}
1 % OGr	2.35 ± 0.31^{N}	2.34 ± 0.04
3 % OGr	2.32 ± 0.31	2.30 ± 0.27
Resin HC (0 %)	2.22 ± 0.80	$2.18 \pm 0.97^{B,C,I,N}$
0.5 % β-AgVO$_3$	$2.10 \pm 0.20^{A,G,L}$	$2.11 \pm 0.49^{A,B,H,O}$
1 % β-AgVO$_3$	$1.78 \pm 0.43^{B,H,J}$	$1.76 \pm 0.38^{D,J,L}$
3 % β-AgVO$_3$	$1.60 \pm 0.31^{B,I,K}$	$1.60 \pm 0.65^{D,K,M}$
0.5 % OGr	$2.13 \pm 0.31^{A,M,O}$	$2.15 \pm 0.46^{A,C}$
1 % OGr	2.33 ± 0.34^{N}	2.28 ± 0.60
3 % OGr	2.30 ± 0.22	2.30 ± 0.10

Legend: One-way ANOVA and post-hoc Tukey ($p < 0.05$). The same capital letters indicate statistical similarity among lines for the different tests.

3.5.6. Color evaluation

A color change was observed for the SC and HC groups containing β-AgVO$_3$ and rGO ($P < 0.05$) (Fig. 11). The highest color change was observed for 3 % rGO ($P = 0.000$) and similarly for 0.5 % and 1 % rGO ($P < 0.05$). SC groups showed a higher color change with the addition of β-AgVO$_3$ and rGO than HC ($P < 0.05$), except for 3 % rGO for HC, which showed a higher color change compared to the other groups ($P < 0.05$).

4. Discussion

The development of innovative dental materials that present antimicrobial activity and maintain their clinical performance is an innovative approach to improving oral health. In this study, correlations were established between the structure and physico-chemical, mechanical, and microbiological properties of SC and HC acrylic resins modified with β-AgVO$_3$ and rGO. Among the concentrations evaluated (0.5, 1, and 3 %), only β-AgVO$_3$ showed a MIC effective against *C. albicans*, *P. aeruginosa*, *S. aureus*, and *S. mutans*. While previous studies have demonstrated the antimicrobial properties of graphene compounds [7,16], the current study did not observe a significant reduction in CFU count for rGO samples ($P > 0.05$). These results can be attributed to the lower production of reactive oxygen species (ROS) due to the reduced amount of oxygen (O) present in rGO. Oxygen is known to be responsible for promoting damage to the bacterial cell membrane [18]. By correlating the microbiological results with the SEM images (Fig. 4), it was determined that the direct contact mechanism of rGO was also ineffective. This inefficiency can be attributed to the method of incorporating the material into the acrylic powder and to the nature of the agglomerates arranged on the rGO TEM images, which hindered the dispersion of the graphene sheets over the entire surface of the sample.

A potential increase in the accumulation of microorganisms was observed for the rGO groups compared to the β-AgVO$_3$ groups, although this observation did not reach statistical significance ($P > 0.05$). This trend was observed based on changes in the sorption,

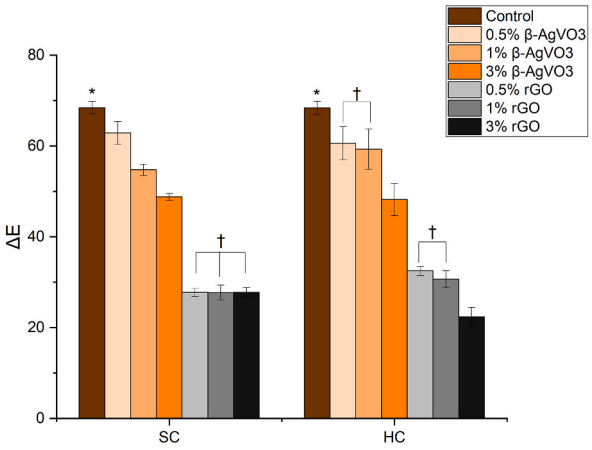

Fig. 11. Mean values and standard deviation of color change (ΔE) of acrylic resins incorporated with rGO and β-AgVO$_3$. Legend: * statistical difference for all groups and † similarity between the indicated groups.

solubility, roughness, and porosity of the resins. Despite the statistical similarity, these results may contribute to bacterial adhesion and colonization. In addition, these results corroborate the electrostatic state observed from the wettability. Although the surface of the resins became more hydrophilic with the addition of rGO, there were no significant changes in contact angles (angles less than 90°). These results suggest that the enhanced adhesion of *P. aeruginosa*, *S. aureus*, and *S. mutans* is attributed to the binding of the bacteria to the attachment substrate, which is dependent on physicochemical surface parameters, including both micro- and macroadhesive structures [31,47].

Resins containing β-$AgVO_3$ show antimicrobial activity proportional to the incorporated concentration, according to previous results [20]. In this study, similar antimicrobial activity was observed as previously reported [20]. However, 0.5 % and 3 % β-$AgVO_3$ HC samples showed low antimicrobial activity due to the formation of small agglomerates of the material (Fig. 7). Higher antimicrobial efficacy against *C. albicans* and *S. mutans* was observed for 1 % β-$AgVO_3$ HC samples. Agglomeration of nanoparticles occurs due to their encapsulation in the polymer matrix. This phenomenon is mediated by van der Waals forces and electrostatic attraction, which prevent the homogeneous distribution of β-$AgVO_3$ and its antimicrobial activity.

The reduction in CFU can be correlated with the surface roughness results, the decrease in the contact angle of the sessile drop with the surface of the samples, and the decrease in sorption, solubility, and porosity. The microbial reduction can be attributed to the synergy between the mechanisms of action of β-$AgVO_3$ and the surface modifications of the samples [47]. Surface modifications such as reduced hydrophilicity, negative charge, and the absence of structural defects contribute to the non-adhesion of microorganisms with positive electrostatic charge [47].

Based on the findings of the microbiological analysis and cell viability, it was concluded that the groups with β-$AgVO_3$ exhibited better antimicrobial efficacy compared to those with rGO. This difference can be attributed to the incorporation method and the specific graphene compound used (rGO). The lower amount of O_2 present in this compound and its aggregate structure may have reduced its antimicrobial activity. For future studies, it is recommended to explore alternative methods of incorporation and to investigate graphene compounds in their oxidized forms.

In this study, the incorporation of nanomaterials into acrylic resins aimed to increase antimicrobial activity without affecting mechanical properties such as flexural strength and hardness. These evaluations were critical to ensuring that the modified material maintained its performance and microbiological activity without compromising its mechanical properties.

The flexural strength of the resins with β-$AgVO_3$ was adequate (65 MPa) according to the ISO 1567 standard. Maintaining this property contributes to the clinical success of this material. The flexural strength of SC resins containing rGO increased proportionally with the concentration of the compound. The best results were observed for 0.5 % rGO compared to the other groups ($P < 0.05$). In contrast, HC resins containing rGO showed lower flexural strength results due to the heating of the nanomaterial during polymerization [48]. Graphene compounds exposed to high temperatures can show movement of their atoms and impairment of their crystalline structure [48]. In addition, they can exhibit structural defects due to their high reactivity to heat [48].

The addition of β-$AgVO_3$, as seen above, maintained its values for mechanical properties. In terms of hardness, the same results were obtained for both resins compared (SC and HC). The incorporation of rGO improved the hardness of both SC and HC resins. Agarwalla, Malhotra, and Rosa [49] reported that graphene composites used to reinforce polymers showed minimal improvement in hardness. This is attributed to the challenge of forming chemical bonds between the graphene and the polymer chain [15,49]. However, the observed changes may not be clinically significant [15,49]. Furthermore, the addition of rGO significantly changed the color of the SC and HC resins due to their black color. This color change is unacceptable for oral application [46].

After correlating the structure of the materials and their properties, the need to study methods for incorporating nanoparticles and their chemical interaction with the polymer matrix was observed. These proposals will contribute to the development of polymeric materials that exhibit antimicrobial activity and maintain or improve their mechanical properties. It will also help to understand the performance of the modified material and its impact on clinical practice. Thus, the accumulation of oral pathogenic microorganisms can be reduced, and the material can withstand the mechanical challenges of the oral cavity.

5. Conclusion

Based on the results of this research, it can be inferred that.

- The addition of 3 % β-$AgVO_3$ in SC and HC showed better results against *C. albicans* and *P. aeruginosa.* The addition of rGO in SC and HC induced higher biofilm accumulation of *S. mutans* and *P. aeruginosa.*
- The physicochemical properties (roughness, sorption, solubility, porosity, and color) were favored for the β-$AgVO_3$ groups of SC and HC resins. The addition of rGO increased the wettability of SC.
- The mechanical properties were maintained with the addition of β-$AgVO_3$ for SC and HC, with HC showing better mechanical properties than SC.
- The addition of rGO in SC showed higher flexural strength compared to the other SC and HC groups. The addition of rGO increased hardness for SC and HC, with higher values for HC.

Data availability statement

Data will be made available on request.

CRediT authorship contribution statement

Beatriz Danieletto Sahm: Writing – original draft, Methodology, Investigation, Formal analysis, Data curation, Conceptualization. **Izabela Ferreira:** Writing – original draft, Methodology, Investigation, Formal analysis, Data curation, Conceptualization. **João Marcos Carvalho-Silva:** Writing – review & editing, Writing – original draft, Visualization, Methodology, Formal analysis, Conceptualization. **Ana Beatriz Vilela Teixeira:** Writing – original draft, Methodology, Data curation. **Jean Valdir Uchôa Teixeira:** Writing – original draft, Methodology. **Paulo Noronha Lisboa-Filho:** Writing – original draft, Methodology, Formal analysis. **Oswaldo Luiz Alves:** Resources. **Andréa Cândido dos Reis:** Writing – review & editing, Visualization, Validation, Supervision, Resources, Project administration, Methodology, Investigation, Funding acquisition, Formal analysis, Data curation, Conceptualization.

Declaration of competing interest

The authors declare that they have no known competing financial interests or personal relationships that could have appeared to influence the work reported in this paper.

Acknowledgements

We thank the São Paulo Research Foundation (FAPESP) for funding this study (grant 2022/01344-4). We thank the Oral Rehabilitation Research Laboratory FORP/USP, Dentistry Research Laboratory FORP/USP, and Center for Development of Functional Materials (CDM) for the facilities.

References

[1] C. Bacali, I. Baldea, M. Moldovan, R. Carpa, D.E. Olteanu, G.A. Filip, V. Nastase, L. Lascu, M. Badea, M. Constantiniuc, F. Badea, Flexural strength, biocompatibility, and antimicrobial activity of a polymethyl methacrylate denture resin enhanced with graphene and silver nanoparticles, Clin Oral Investig 24 (8) (2020 Aug) 2713–2725.
[2] N. Jiang, P. Tan, M. He, J. Zhang, D. Sun, S. Zhu, Graphene reinforced polyether ether ketone nanocomposites for bone repair applications, Polym. Test. (2021) 1–11.
[3] A.B.V. Teixeira, C.L. Vidal, D.T. de Castro, C. de Oliveira-Santos, M.A. Schiavon, A.C. Dos Reis, Incorporating antimicrobial nanomaterial and its effect on the antimicrobial activity, flow and radiopacity of endodontic sealers, Eur Endod J 2 (2017) 1–6.
[4] I. Ferreira, C.L. Vidal, A.L. Botelho, et al., Effect of nanomaterial incorporation on the mechanical and microbiological properties of dental porcelain, J. Prosthet. Dent 123 (2020) 529.
[5] L.M. Uehara, I. Ferreira, A.L. Botelho, M.L.D.C. Valente, A.C.D. Reis, Influence of β-AgVO3 nanomaterial incorporation on mechanical and microbiological properties of dental porcelain, Dent. Mater. 38 (2022) e174–e180.
[6] M.R. de Campos, A.L. Botelho, A.C. Dos Reis, Nanostructured silver vanadate decorated with silver particles and their applicability in dental materials: a scope review, Heliyon 7 (6) (2021) e07168, 1-7.
[7] P. Kumar, P. Huo, R. Zhang, B. Liu, Antibacterial properties of graphene-based nanomaterials, Nanomaterials 9 (2019) 737.
[8] K. Walczak, G. Schierz, S. Basche, C. Petto, K. Boening, M. Wieckiewicz, Antifungal and surface properties of chitosan-salts modified PMMA denture base material, Molecules 25 (24) (2020 Dec 13) 5899, 1.
[9] M. Menini, P. Pesce, F. Pera, F. Barberis, A. Lagazzo, L. Bertola, P. Pera, Biological and mechanical characterization of carbon fiber frameworks for dental implant applications, Mater. Sci. Eng., C 70 (Pt 1) (2017 Jan 1) 646–655.
[10] I.X. Yin, J. Zhang, I.S. Zhao, M.L. Mei, Q. Li, C.H. Chu, The antibacterial mechanism of silver nanoparticles and its application in dentistry, Int. J. Nanomed. 15 (2020 Apr 17) 2555–2562.
[11] E. Sánchez-López, D. Gomes, G. Esteruelas, L. Bonilla, A.L. Lopez-Machado, R. Galindo, A. Cano, M. Espina, M. Ettcheto, A. Camins, A.M. Silva, A. Durazzo, A. Santini, M.L. Garcia, E.B. Souto, Metal-based nanoparticles as antimicrobial agents: an overview, Nanomaterials 10 (2) (2020 Feb 9) 292.
[12] J.M. Silva, A.B. Teixeira, A.C. Reis, Silver-based gels for oral and skin infections: antimicrobial effect and physicochemical stability, Future Microbiol. 18 (2023 Sep) 985–996, https://doi.org/10.2217/fmb-2023-0034.
[13] R.D. Holtz, A.G. Souza Filho, M. Brocchi, D. Martins, N. Durán, O.L. Alves, Development of nanostructured silver vanadates decorated with silver nanoparticles as a novel antibacterial agent, Nanotechnology 21 (18) (2010 May 7) 185102, https://doi.org/10.1088/0957-4484/21/18/185102.
[14] R.D. Holtz, B.A. Lima, A.G. Souza Filho, M. Brocchi, O.L. Alves, Nanostructured silver vanadate as a promising antibacterial additive to water-based paints, Nanomedicine 8 (6) (2012 Aug) 935–940, https://doi.org/10.1016/j.nano.2011.11.012.
[15] J.H. Lee, J.K. Jo, D.A. Kim, K.D. Patel, H.W. Kim, H.H. Lee, Nano-graphene oxide incorporated into PMMA resin to prevent microbial adhesion, Dent. Mater. 34 (4) (2018) e63–e72.
[16] A. Radhi, D. Mohamad, F.S. Rahman, A.M. Abdullah, H. Hasan, Mechanism and factors influence of graphene-based nanomaterials antimicrobial activities and application in dentistry, J. Mater. Res. Technol. 11 (2021) 1290–1307.
[17] S. Park, H. Kim, K.S. Choi, M.K. Ji, S. Kim, Y. Gwon, C. Park, J. Kim, H.P. Lim, Graphene–chitosan hybrid dental implants with enhanced antibacterial and cell-proliferation properties, Appl. Sci. 10 (2020) 4888.
[18] T. Seifi, A.R. Kamali, Anti-pathogenic activity of graphene nanomaterials: a review, Colloids Surf. B Biointerfaces 199 (2021) 111509.
[19] D.T. Castro, A.B.V. Teixeira, O.L. Alves, A.C. dos Reis, Cytotoxicity and elemental release of dental acrylic resin modified with silver and vanadium based antimicrobial nanomaterial, Health Sci. 23 (1) (2021) 12–17.
[20] D.T. Castro, M.L. Valente, C.H. da Silva, et al., Evaluation of antibiofilm and mechanical properties of new nanocomposites based on acrylic resins and silver vanadate nanoparticles, Arch. Oral Biol. 67 (2016) 46–53.
[21] J.V.U. Teixeira, G.J.C. Pimentel, A.A. Santos, L.F.G. Dias, V.R. Mastelaro, P.N. Lisboa-Filho, Partially reduced graphene oxide produced by glucose in alkaline conditions using probe sonication: the role of the base in reduction, J. Mater. Res. Technol. 26 (2023) 1785–1797, https://doi.org/10.1016/j.jmrt.2023.07.211.
[22] Z. Bytešníková, M. Koláčková, M. Dobešová, P. Švec, A. Ridošková, J. Pekárková, J. Přibyl, P. Cápal, D. Húska, V. Adam, L. Richtera, New insight into the biocompatibility/toxicity of graphene oxides and their reduced forms on *Chlamydomonas reinhardtii*, NanoImpact 31 (2023) 100468, https://doi.org/10.1016/j.impact.2023.100468.
[23] C. Kong, J. Chen, P. Li, Y. Wu, G. Zhang, B. Sang, R. Li, Y. Shi, X. Cui, T. Zhou, Respiratory toxicology of graphene-based nanomaterials: a review, Toxics 12 (1) (2024) 82, https://doi.org/10.3390/toxics12010082.
[24] A.B.V. Teixeira, D.T. de Castro, M.A. Schiavon, A.C. Dos Reis, Cytotoxicity and release ions of endodontic sealers incorporated with a silver and vanadium base nanomaterial, Odontology 108 (4) (2020) 661–668, https://doi.org/10.1007/s10266-020-00507-x.

[25] S.R.U. Rehman, R. Augustine, A.A. Zahid, R. Ahmed, M. Tariq, A. Hasan, Reduced graphene oxide incorporated GelMA hydrogel promotes angiogenesis for wound healing applications, Int. J. Nanomed. 14 (2019) 9603–9617, https://doi.org/10.2147/IJN.S218120.
[26] N. Bellier, P. Baipaywad, N. Ryu, J.Y. Lee, H. Park, Recent biomedical advancements in graphene oxide- and reduced graphene oxide-based nanocomposite nanocarriers, Biomater. Res. 26 (1) (2022) 65, https://doi.org/10.1186/s40824-022-00313-2.
[27] C. Liao, Y. Li, S.C. Tjong, Graphene nanomaterials: synthesis, biocompatibility, and cytotoxicity, Int. J. Mol. Sci. 19 (11) (2018) 3564, https://doi.org/10.3390/ijms19113564.
[28] U. Mangal, J.Y. Kim, J.Y. Seo, J.S. Kwon, S.H. Choi, Novel poly(methyl methacrylate) containing nanodiamond to improve the mechanical properties and fungal resistance, Materials 12 (20) (2019 Oct 21) 3438.
[29] D. Rokaya, V. Srimaneepong, J. Sapkota, J. Qin, K. Siraleartmukul, V. Siriwongrungson, Polymeric materials and films in dentistry: an overview, J. Adv. Res. 14 (2018 May 3) 25–34.
[30] M.S. Zafar, Prosthodontic applications of polymethyl methacrylate (PMMA): an update, Polymers 12 (10) (2020 Oct 8) 2299.
[31] B.D. Sahm, A.L. Botelho, J.A.M. Agnelli, A.C. Reis, Relation of physicochemical properties and accumulation of microorganisms in acrylic resins with antimicrobial properties: a systematic review, Polym. Bull. 79 (2022) 1–13.
[32] J.M. Carvalho-Silva, C.S. Gaspar, A.C. Dos Reis, A.B.V. Teixeira, Denture stomatitis: treatment with antimicrobial drugs or antifungal gels? A systematic review of clinical trials, J. Prosthet. Dent 3913 (23) (2024), https://doi.org/10.1016/j.prosdent.2023.12.014, 00829-6.
[33] L.M. Schlecht, B.M. Peters, B.P. Krom, J.A. Freiberg, G.M. Hänsch, S.G. Filler, M.A. Jabra-Rizk, M.E. Shirtliff, Systemic Staphylococcus aureus infection mediated by Candida albicans hyphal invasion of mucosal tissue, Microbiology 161 (2015) 168–181, https://doi.org/10.1099/mic.0.083485-0.
[34] R. Fourie, C.H. Pohl, Beyond antagonism: the interaction between Candida species and Pseudomonas aeruginosa, J Fungi (Basel) 5 (2019) 1–18, https://doi.org/10.3390/jof5020034.
[35] L.J. Kahl, N. Stremmel, M.A. Esparza-Mora, R.M. Wheatley, R.C. MacLean, M. Ralser, Interkingdom interactions between Pseudomonas aeruginosa and Candida albicans affect clinical outcomes and antimicrobial responses, Curr. Opin. Microbiol. 75 (2023) 102368, https://doi.org/10.1016/j.mib.2023.102368.
[36] A.G. Paleari, J. Marra, A.C. Pero, L.S. Rodriguez, A. Ruvolo-Filho, M.A. Compagnoni, Effect of incorporation of 2-tert-butylaminoethyl methacrylate on flexural strength of a denture base acrylic resin, J. Appl. Oral Sci. 19 (3) (2011) 195–199.
[37] Z. Wang, Y. Shen, M. Haapasalo, Dental materials with antibiofilm properties, Dent. Mater. 30 (2) (2014) e1–e16.
[38] L. Chen, B.I. Suh, J. Yang, Antibacterial dental restorative materials: a review, Am. J. Dent. 31 (Sp Is B) (2018) 6B–12B.
[39] Y. Wang, S. Costin, J.F. Zhang, et al., Synthesis, antibacterial activity, and biocompatibility of new antibacterial dental monomers, Am. J. Dent. 31 (Sp Is B) (2018) 17B–23B.
[40] M. Gu, L. Lv, F. Du, T. Niu, T. Chen, D. Xia, S. Wang, X. Zhao, J. Liu, Y. Liu, C. Xiong, Effects of thermal treatment on the adhesion strength and osteoinductive activity of single-layer graphene sheets on titanium substrates, Sci. Rep. 8 (2018) 1–5.
[41] S. Kreve, V.C. Oliveira, L. Bachmann, O.L. Alves, A.C.D. Reis, Influence of AgVO3 incorporation on antimicrobial properties, hardness, roughness and adhesion of a soft denture liner, Sci. Rep. 9 (1) (2019) 1–9.
[42] W. Qin, Y. Li, J. Ma, Q. Liang, X. Cui, H. Jia, B. Tang, Osseointegration and biosafety of graphene oxide wrapped porous CF/PEEK composites as implantable materials: the role of surface structure and chemistry, Dent. Mater. 36 (2020) 1289–1302, https://doi.org/10.1016/j.dental.2020.06.004.
[43] R.K. Matharu, A.T. Tabish, T. Trakoolwilaiwan, J. Mansfield, J. Moger, T. Wu, C. Lourenço, B. Chen, L. Ciric, I.P. Parkin, M. Edirisinghe, Microstructure and antibacterial efficacy of graphene oxide nanocomposite fibres, J. Colloid Interface Sci. 571 (2020) 239–252.
[44] S. Abdolhosseinzadeh, H. Asgharzadeh, H. Seop Kim, Fast and fully-scalable synthesis of reduced graphene oxide, Sci. Rep. 5 (2015 May 15) 10160.
[45] P. Khaki, A. Sharma, P. Bhalla, Comparison of two disc diffusion methods with minimum inhibitory concentration for antimicrobial susceptibility testing of *Neisseria gonorrhoeae* isolates, Ann. Med. Health Sci. Res. 4 (3) (2014) 453–456, https://doi.org/10.4103/2141-9248.133477.
[46] D. Möbius, A. Braun, R. Franzen, Evaluation of tooth color change after a bleaching process with different lasers, Odontology 17 (2024), https://doi.org/10.1007/s10266-023-00886-x.
[47] S. Kreve, A.C.D. Reis, Bacterial adhesion to biomaterials: what regulates this attachment? A review, Jpn Dent Sci Rev. 57 (2021 Nov) 85–96.
[48] M. Tahriri, M. Del Monico, A. Moghanian, M. Tavakkoli Yaraki, R. Torres, A. Yadegari, L. Tayebi, Graphene and its derivatives: opportunities and challenges in dentistry, Mater. Sci. Eng., C 102 (2019 Sep) 171–185.
[49] S.V. Agarwalla, R. Malhotra, V. Rosa, Translucency, hardness and strength parameters of PMMA resin containing graphene-like material for CAD/CAM restorations, J. Mech. Behav. Biomed. Mater. 100 (2019 Dec) 103388.